

MEASUREMENT OF THE FLOW AROUND THE SUBMERGED VORTEX CAVITATION IN A PUMP INTAKE BY MEANS OF PIV

Takahide NAGAHARA, Toshiyuki SATO, Tomoyoshi OKAMURA
Research & Development Laboratory
Hitachi Industries Co., Ltd.
603 Kandatsu-machi, Tsuchiura-shi, Ibaraki 300-0013 Japan
E-mail: takahide_nagahara@gm.hitachi-hic.jp

Ryuichiro IWANO
Power & Industrial Systems R & D Lab., Hitachi Ltd., Japan

ABSTRACT

The flow structure of the vortex occurring in a pump suction intake sump has been investigated and the accuracy of CFD calculation predicting vortex cavitation evaluated experimentally by using particle image velocimetry to measure the flow around the vortex. The test apparatus consisting of the model suction intake and the pressure tank could control the mean inlet velocity, the circulation, and the pressure at the pump intake bell mouth. Vortices of various strengths were generated using this apparatus, and velocity fields around them were measured and compared — with respect to the velocity distribution, the circulation, and the core radius — with the corresponding fields obtained by CFD calculation. The results of those comparisons and the difference between the instantaneous and time-averaged velocity profiles are described and discussed.

INTRODUCTION

When construction costs are reduced by using smaller pump stations for power plants and drainage stations, the mean flow velocity at the pump suction intake increases and this increases the potential for submerged vortex cavitation and air entraining vortices. Because these kinds of strong vortices cause vibration and noise in pumps, reliable and trouble-free operation can be assured by designing a suction configuration that prevents the occurrence of these vortices.

Designs for vortex-free intake configurations have been evaluated by using scale models, and there are many papers reporting investigations and observations of the various vortices occurring in suction intakes (see, *e.g.*, [1]). Because of the high experimental cost and the large amount of manufacturing time needed to make these models, however, CFD calculation has recently begun to be used to evaluate the flow around the suction intake in pumps. CFD reduces the number of experimental tests needed, but the accuracy of the calculation result has sometimes been suspect.

Rajendran *et al.* [2,3] reported that the numerically simulated flow field around the intake sump of a model pump was in good agreement with the one measured by particle imaging velocimetry (PIV). Shibata *et al.* [4-6] described a new method of predicting submerged vortices that uses CFD with a vortex model and compared the predicted critical velocity for submerged vortex cavitation with the critical velocity measured experimentally. The essential characteristic of this method is its use of the vortex model to compensate the lack of the resolution in the numerical calculation around the vortex center. The prediction occurrences of submerged cavitation were in agreement with the ones observed experimentally. On the other hand, we previously investigated the effect of the occurrence of submerged vortices on the hydraulic forces of the pump impeller [7]. In that work we compared the calculated velocity distribution around the submerged vortices with the distribution measured using particle tracking velocimetry (PTV).

There is, however, no quantitative data concerning the detailed velocity profiles around the vortex with and without cavitation. Moreover there is few report of the comparison of measured and CFD results with regard to the submerged vortex cavitation. Such data and such a comparison would make it possible to design the pump suction intake configuration for trouble-free operation without the experimental evaluation.

In the research reported here we therefore used PIV to measure the detailed velocity distribution around the submerged vortex cavitation and compared the results with the velocity field calculated by CFD.

NOMENCLATURE

D_b = pump bell mouth diameter
 H_b = height from the channel floor to the pump bell
 P = static pressure in the channel
 P_0 = atmospheric pressure
 r_c = cavitation core radius
 R_e = Reynolds number

- U_{xy} = velocity component in the x-direction along y-axis
- U_{yx} = velocity component in the y-direction along x-axis
- V = mean approach velocity of the intake channel
- V_r = velocity ratio
- Γ = circulation

EXPERIMENTAL APPARATUS

The experimental equipment and the observation area of the submerged vortex occurring in the lower part of the pump bell are shown schematically in Fig. 1. The experimental equipment had a pressure tank that can control the pump inlet pressure, also cavitation number. A gauge pressure transmitter was connected to the pressure tank to measure the static pressure.

The rectangular channel of the intake was divided into two sections by the center pier upstream region of the pump suction sump, and two valves and circulating pumps were connected to the approach pipes. The flow rate of each channel was controlled by adjusting the speed of each circulating pump or opening the valves and was measured by electromagnetic flow meters in the return circuit.

The mean velocity and the swirl flow at the lower part of the pump inlet, which causes the submerged vortex cavitation, could thus be changed at will. The intake channel was filled with water and had no free surface except that in the upper part of the pressure tank.

An acrylic resin window was installed in the wall around the model pump, which was also made of acrylic resin. The model pump had no impeller and represented only the outside configuration of the typical prototype pump.

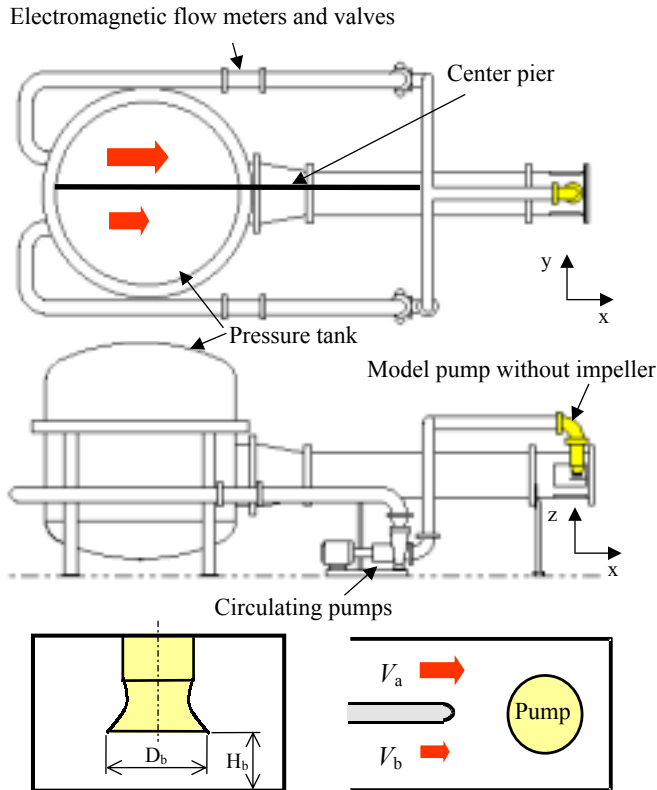


Fig. 1 Schematic diagram of the experimental equipment

The experiment was done using the following configuration parameter: height from the bottom to the bell, normalized with respect to the bell diameter: $H_b/D_b=0.5$. The Reynolds number, estimated from the pump bell diameter D_b and the mean velocity at the bell, was of the order of 10^5 .

PIV MEASUREMENT SYSTEM

The PIV measurement system consisted of a double-pulsed Nd-Yag laser; a high-resolution, high-frame-rate cross-correlation CCD camera; a synchronizer; and data analysis software. The PIV system and the model pump intake are shown schematically in Fig. 2. A laser light sheet was provided, through a cylindrical lens, from the outside of the suction intake back-wall window and illuminated the measuring section parallel to the channel floor in the lower part of the model pump. As shown in Fig 2, the measured velocity field around the vortex was $0.25D_b$ above the channel floor. The cross-correlation camera recording the particle images of the vortex section was placed under the intake channel near the model pump. The power of the laser was very high (maximum 120 mJ), so that very small air bubbles similar to the nuclei naturally in the water reflected enough of the laser light sheet to record good particle images. Therefore, no other particles (for example, made of polystyrene) were used in this research.

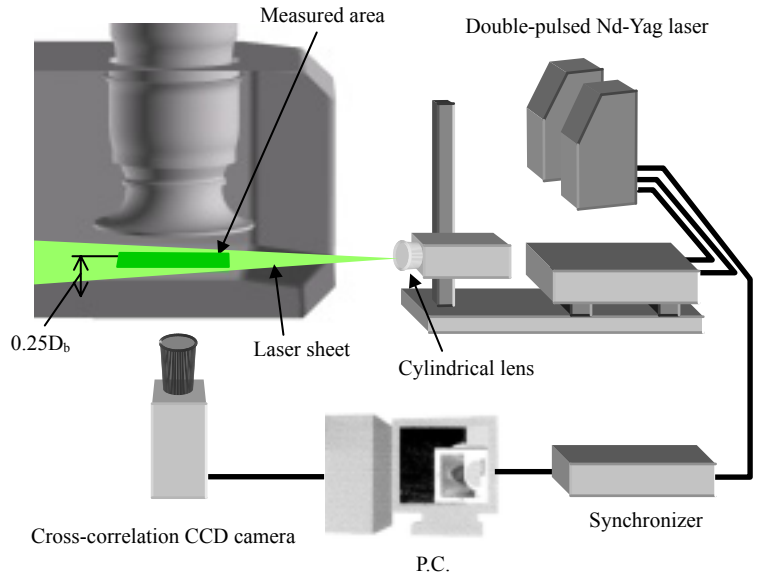


Fig. 2 Schematic diagram of the PIV measurement system

The analysis software used a cross-correlation technique to find the displacement of particles between two images taken at a very short interval. The evaluation area was set to be 32 pixels by 32 pixels (which is equivalent to $0.02D_b$ mm by $0.02D_b$) so that we could obtain as much velocity data in the vortex core area as possible. Pairs of the particle images taken at 0.27-s intervals were evaluated, and the instantaneous velocity field around the vortex was estimated. Finally, both averaged and instantaneous data were obtained.

EXPERIMENTAL CONDITIONS

The experimental conditions are listed in Table 1. The parameters V and V_r respectively denote the mean approach velocity and the ratio of the mean approach velocities of each channel divided by the center pier at the upstream region of the intake channel. That is,

$$V = (V_a + V_b)/2 \quad (1)$$

$$V_r = V_a/(V_a + V_b) \quad (2)$$

The submerged vortices with cavitation core were observed in cases 3 and 4. Thus, the conditions of cases 5 and 6, in which the static pressure was three times what it was in cases 3 and 4, was added in order to eliminate the cavitation occurrence and to compare the flow fields around the vortex with and without cavitation.

Table 1. Experimental conditions.

	V/V_{ref}	V_r	P/P_0
Case 1	1	0.6	1
Case 2	1	0.8	1
Case 3	3	0.6	1
Case 4	3	0.8	1
Case 5	3	0.6	3
Case 6	3	0.8	3

NUMERICAL SIMULATION

The numerical calculations were carried out by means of a CFD code that uses a cell-centered finite volume method to solve the Reynolds-averaged Navier-Stokes (RANS) equations with the RNG $k-\epsilon$ turbulence model. Approximately 1,000,000 points, including the suction intake and the model pump configuration, were generated in this calculation. The prescribed velocity and the pressure conditions were respectively applied at the inlet and outlet boundaries. The distance between the pump and the inlet boundary was provided as approximately $15D_b$. The calculations were implemented under the conditions of case 1, 2, 5, and 6 shown in Table 1 as single-phase and incompressible flow simulations.

The measurement circulation of the vortices was compared with that calculated using the method described in Refs. [4–6]. This method was developed for the purpose of predicting the inception of the submerged vortex cavitation. In the process of the prediction, the circulation and the axial velocity gradient were calculated along the analytically identified vortex portion by using the global flow field from the CFD calculation result. This technique was applied to settle the integral path c and the circulation of the submerged vortices was calculated using the following formula.

$$\Gamma = \oint_c \mathbf{u} \cdot d\mathbf{s} \quad (3)$$

RESULTS AND DISCUSSION

OBSERVED SUBMERGED VORTEX CAVITATION

Submerged vortex cavitation observed in the lower part of the model pump in cases 3 and 4 is shown in Fig. 3. The submerged vortices were generated at the floor of the channel to the model pump inlet and existed continuously in both cases, but the diameter of the cavitation area at the vortex center was larger in case 4. This difference was mainly due to the swirl flow strength increasing because of the velocity distortion upstream. Of course, these cavitation cores caused by the strong vortices were generated intentionally for the purpose of this research. In the actual design of a prototype pump, they will be eliminated by using a splitter plate installed on the floor. Moreover, as described in Ref. 5, the critical velocity of the vortex cavitation inception will also be increased.

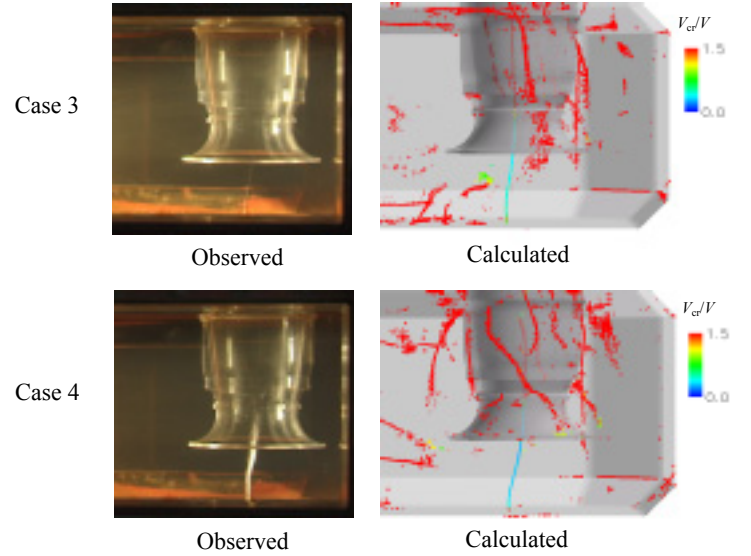


Fig. 3 Observed submerged vortex cavitation compared with that predicted by CFD calculation

The submerged vortices predicted using CFD and the method described in Refs. [4–6] are shown, along with the observed vortices, in Fig. 3. The vortex filaments for which the value of V_{cr}/V is less than 1.0 are vortex portions that can cause submerged vortex cavitation. The experimental and calculated results agree well with regard to the shape and position of the cavitation vortices.

VELOCITY FIELD AROUND THE VORTEX

The measurement and CFD results for the velocity magnitude contour around the vortices are shown in Fig. 4. The measurement results are the time-averaged velocities of the 100 instantaneous data obtained using PIV. The velocity profile of the swirl flow around the one vortex center were measured and calculated in each condition. The tangential velocity distribution around the vortex increased in proportion as V or V_r increased. The positions of the vortex centers differed slightly between the measured and calculated results.

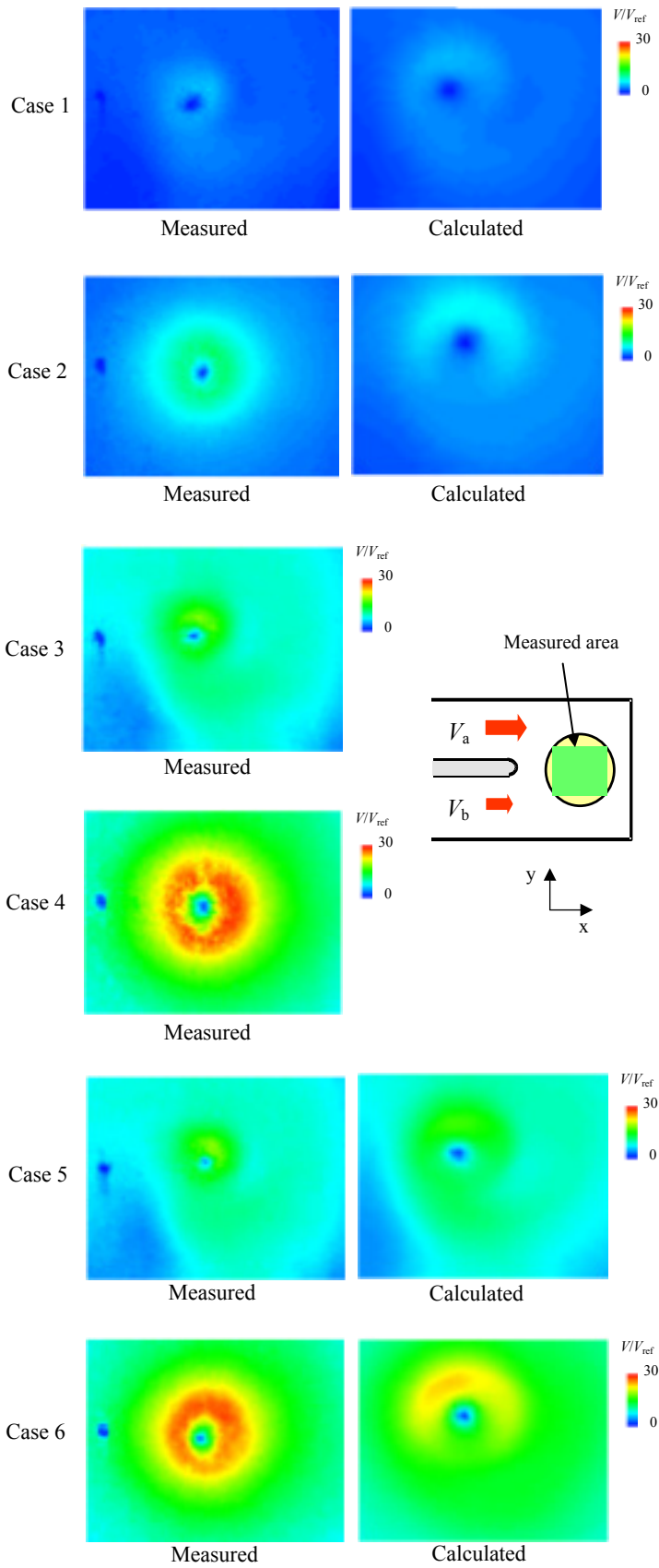


Fig. 4 Velocity magnitude contour of the measurement and CFD results

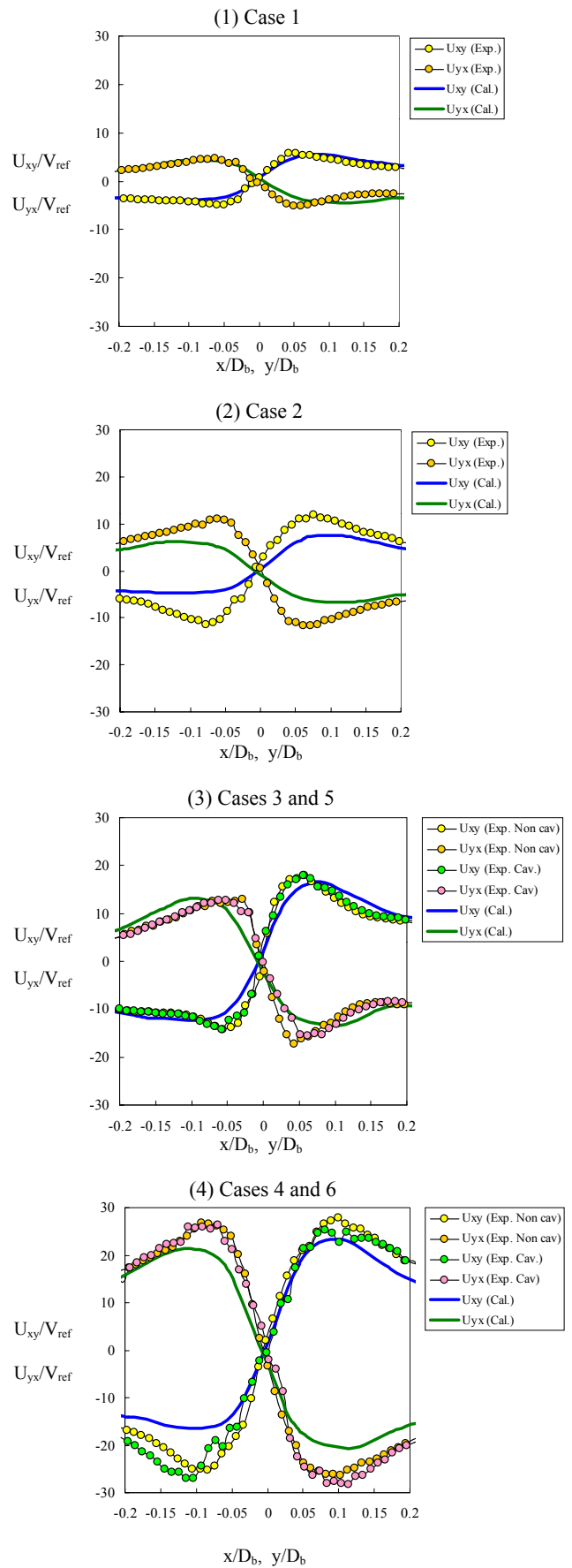


Fig. 5 Comparison of the tangential velocity profiles

The velocity components U_{xy} and U_{yx} (respectively along the local y and x coordinate axes whose origins are set at each vortex center) are shown in Fig. 5. The velocity profile including the maximum tangential velocity calculated under $V_r = 0.6$ conditions (cases 1 and 3) were good agreement with the experimental result when the mean approach velocity V/V_{ref} was 1 or 3. The calculated core radii were slightly larger than the experimental ones. On the other hand, when $V_r = 0.8$ (cases 2 and 6) and no vortex cavitation was observed, the calculated maximum velocities were lower than the experimental ones. The reason for these differences is not clear. It appears that this blunt velocity profile was caused by the excessive increase in the turbulence or numerical viscosity calculated because of the difference of the flow field — especially strength of the swirl flow— between $V_r = 0.6$ and 0.8.

The velocity profiles measured around the cavitating vortices (cases 3 and 4) are plotted in Fig. 5 for comparison with the profiles around the noncavitating vortices (cases 5 and 6). The maximum velocities and core radii for the cavitating vortices were slightly larger than those for the noncavitating vortices. Under these experimental conditions, the swirl flows were mainly caused by the velocity distortion of the upper flow. This may indicate that the maximum circulation and the total angular momentum of the vortices are held constant regardless of the occurrence of vortex cavitation. Thus, it appears that the velocity profile around the cavitating cores in the vicinity of the vortex center slightly increase compared with the velocity profile of vortices having noncavitating cores in order to compensate the lack of the total angular momentum per unit length in the vortex core because of the cavitation [8]. These variations, however, were very small.

According to the observed vortex cavitation shown in Fig. 3, the vortices moved along the channel floor as Ragendran et al. [2] reported. Figure 6 show the movement of the vortex center, defined as the point of the cavitating vortex center, observed in the PIV measurements. The circles in Fig. 6 indicate the regions including each position of the vortex center throughout the measurement. The diameter of the circle for $V_r = 0.8$ (case 4) is about twice that of the circle for $V_r = 0.6$ (case 3). That is one of the reasons that, for the same mean approach velocity (with regard to the time-averaged velocity profile), the core radii measured when $V_r = 0.8$ were slightly larger than those measured when $V_r = 0.6$.

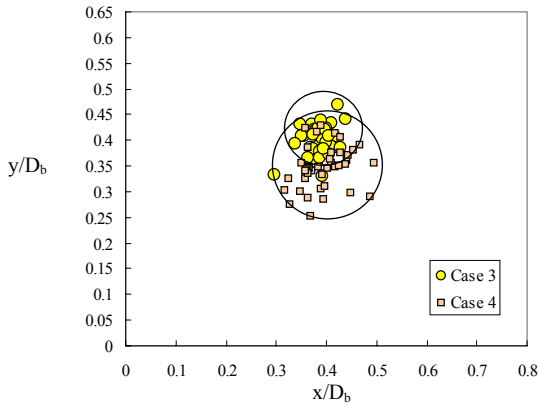


Fig. 6 Movement of the cavitation core

CIRCULATION AND CAVITATION CORE

The technique reported in Refs. [4–6] was used to calculate the circulation of the each vortex from the measured velocity profiles and the velocity profiles obtained by CFD calculation. Figure 7 shows the circulation values for both the time-averaged measurement results and the CFD results. The circulation of the submerged vortex increased in proportion to the increase in V_r and V/V_{ref} , and the circulation calculated from the CFD results roughly agreed with the circulation calculated from the experimental results. For $V_r = 0.6$ the circulation calculated from the CFD results was actually slightly higher than that calculated from the experimental results, and for $V_r = 0.8$ it was slightly lower. This result is the same as the fact presumed from the trend of the velocity profile obtained by both the experiment and the CFD result as shown in Fig. 5. For $V_r = 0.8$, however, although the maximum velocities obtained by the CFD were much lower than the measured ones, the calculated circulations were within 5%. This remarkable fact indicates that the circulation is an accurate parameter for evaluating the vortex strength and that using CFD and the method described in Refs. [4–6] is a very effective way to determine the circulation

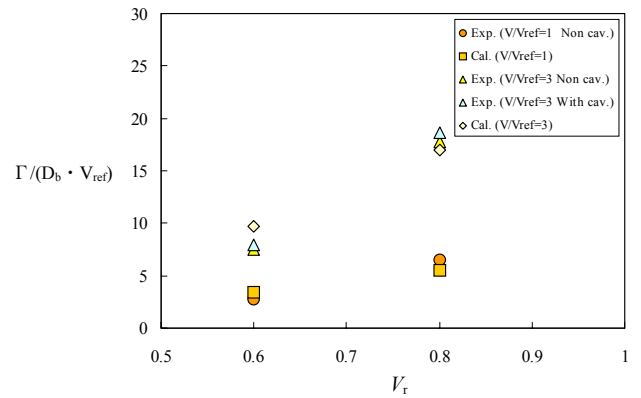


Fig. 7 Comparison of the circulation

Figure 7 also shows the circulation values for vortices with and without the cavitation. As mentioned before, the velocity profiles in the vicinity of a cavitating vortex center were slightly larger than those in the vicinity of a noncavitating one. The circulation values calculated for the cavitating vortices also have the same tendency, being slightly larger than those calculated for the noncavitating ones. The differences were very small, however, (within 5%) even if there was a well-developed cavitating core at the center of the vortex. Moreover, the difference between the measured circulation and the circulation estimated using CFD results was within 5% in case 6. This indicates that the circulation values calculated from the time-averaged values actually measured for submerged vortex cavitation are reasonably equivalent to those calculated from the CFD results. Thus, this technique is adequate for estimating the circulation of the submerged vortex cavitation by using single-phase flow simulation without respect to the multi-phase one.

The variation of the circulation calculated using the velocity profiles measured in cases 3 through 6 in time steps of approximately 2.7 s are shown in Fig. 8. The oscillation of the variation reached about 20% in each case. The corresponding

cavitation core radii measured in images made using the PIV system in cases 3 and 4 are also plotted in Fig. 8. It appears that the variation of the cavitation core radii roughly follows the variation of the circulation. This indicates that the vapor region of the submerged vortex cavitation fluctuates unsteadily with the passage of time and it may expand with the increase in the circulation and shrink with the decrease in the circulation.

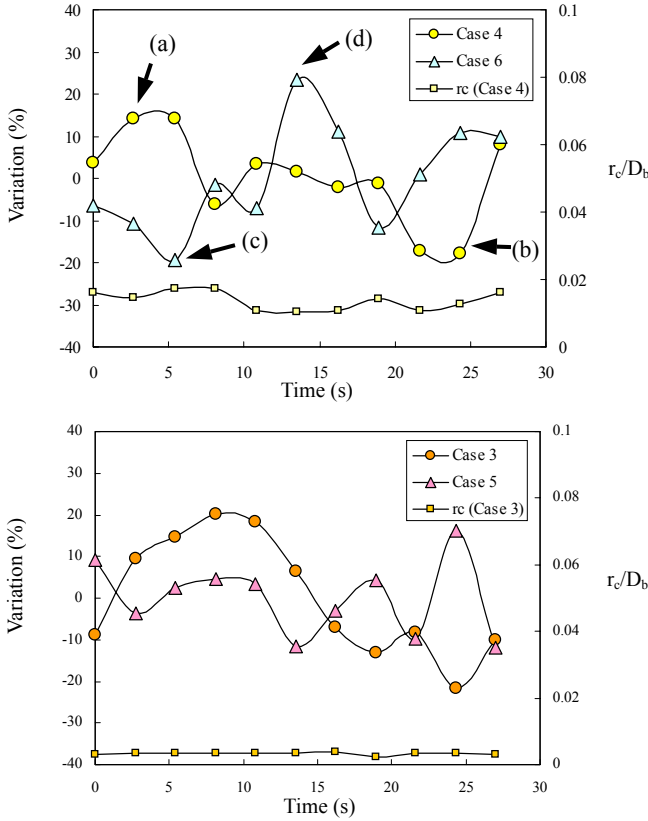


Fig. 8 Variation of the circulation

INSTANTANEOUS AND MEAN STRUCTURES OF VORTICES

Figure 9 shows the instantaneous velocity magnitude contour around the submerged vortex cavitation in cases 4 and 6. The letters below each figure correspond to the points indicated in Fig. 8. In comparison with the time-averaged velocity magnitude contour shown in Fig. 4, the magnitude of the velocities of Fig. 9 in the vicinity of the vortex center are higher and the core regions are very small, too small to be recognized clearly.

The velocity components U_{xy} and U_{yx} for case 6 are shown in Fig. 10 for comparison of the instantaneous velocity profiles and the time-averaged ones. As shown in this figure, the maximum velocities in the instantaneous data are about three times as high as those in the time-averaged data and the core radii are much smaller. This indicates that the velocity profile in the instantaneous data turn becomes blunt, especially for the region in the vicinity of the vortex center, in the time-averaged velocity profile because of the unsteady movement of the vortex center. Therefore, although the CFD steady-state calculation grid was fine enough to divide the vortex center core region to some extent, it seems to be impossible to obtain a maximum-velocities

profile as sharp as that in the instantaneous measurement results owing to the lack of the consideration with unsteadiness.

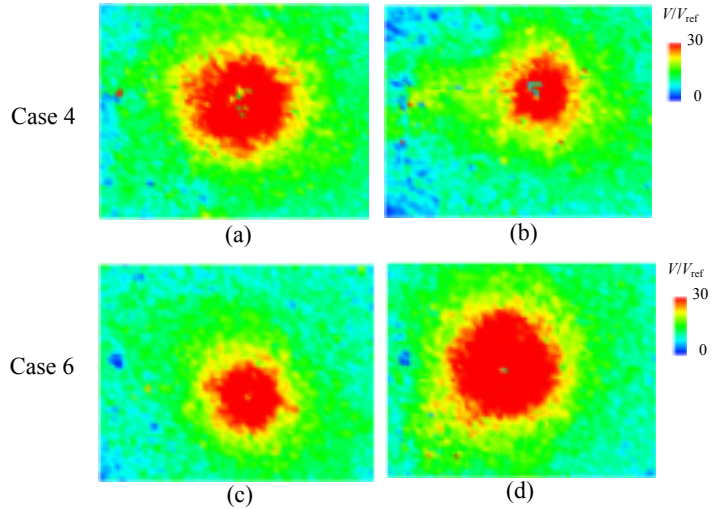


Fig. 9 Velocity magnitude contour of the instantaneous data

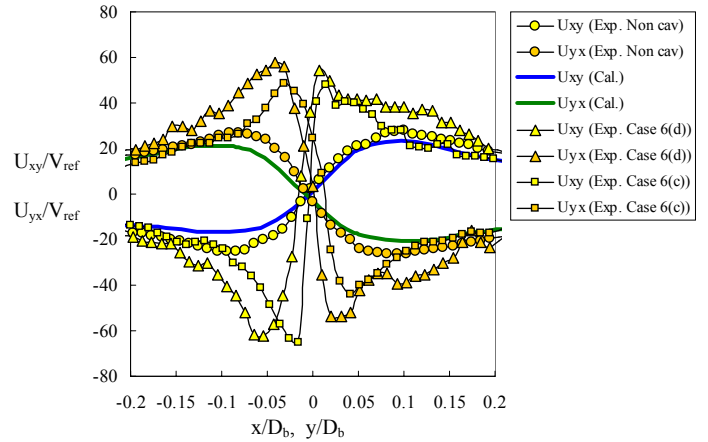


Fig. 10 Comparison of instantaneous velocity

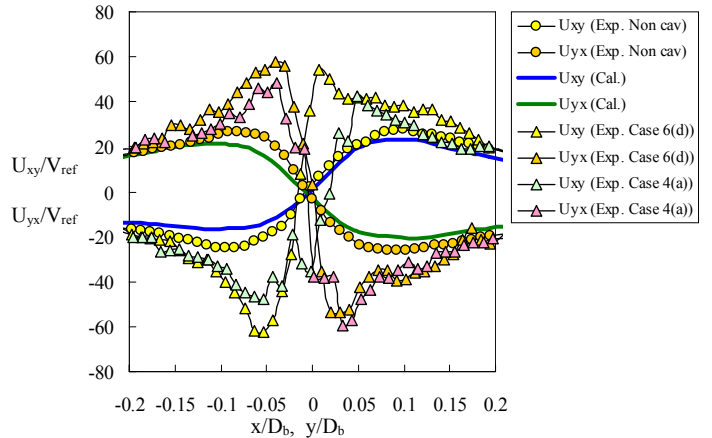


Fig. 11 Comparison of instantaneous velocity profiles with and without cavitation

The instantaneous velocity components around the vortex are compared between cases with and without cavitation (cases 4 and 6) in Fig. 11. The difference is not as clear as in the time-averaged case, because these profiles are examples of instantaneous data picked up from measured data for which the value of circulation fluctuated without any consideration of the comparison criteria, especially with regard to the time-averaging. It seems, however, that the core radii of the cavitating vortex are slightly larger than those of the noncavitating one. This may indicate that the core radius of a cavitating vortex is expanded radially because of the existence of the cavitation core. This is the same trend seen in the comparison of the time-averaged velocity profiles.

CONCLUSIONS

The velocity profiles of the submerged vortices occurring in a pump suction intake with and without cavitation were measured by PIV and compared with the CFD results. The following conclusions were obtained.

- (1) The time-averaged velocity profiles, especially for the maximum velocities around the vortex, measured by PIV are in good agreement with the ones calculated by CFD except when there is large velocity distortion upstream.
- (2) The time-averaged measured velocity profiles and core radii of cavitating vortices are slightly larger than those of noncavitating ones.
- (3) When the circulation values were calculated from both the time-averaged measured data and the CFD result by using the method described in Refs. [4-6], the CFD results roughly agreed with measured ones even though the maximum velocities in the CFD results were much lower than those in the experimental results.
- (4) The circulation of the submerged vortex varies unsteadily and the vapor core radius also varies and roughly follows the variation of the circulation.
- (5) The maximum velocities obtained from instantaneous measurement results are larger than those obtained from time-averaged data and the core radii are much smaller owing to the unsteady movement of the vortex. This may indicate that the steady-state CFD calculation cannot accurately predict the detailed velocity profile in the vicinity of the vortex center even when the computational grid is fine enough to divide the small core region.

ACKNOWLEDGMENTS

We thank Dr. T. Shibata and Mr. H. Shimizu of Hitachi, Ltd. for their valuable advice and discussions. We also thank Mr. K. Yagawa and Mr. H. Takayanagi of T-TEC, Co., Ltd. for their support of our experiments.

REFERENCES

- [1] Ansar, M., and Nakato, T., 1995, "Effect of Cross Flow on Pump-Approach-Flow Distributions at a Pump Intake," *HYDRA 2000* (Vol.2), pp. 114-119.
- [2] Rajendran, V. P., and Patel, V. C., 2000, "Measurement of Vortices in Model Pump-Intake Bay by PIV," *Journal of Hydraulic Eng.*, pp. 322-334.
- [3] Rajendran, V. P., Constantinescu, G. S., and Patel, V. C., 1998, "Experiments on Flow in a Model Water-Pump Intake Sump to Validate a Numerical Model," *ASME FEDSM98-5098*.
- [4] Shibata, T., Iwano, R., Nagahara, T., and Okamura, T., 2000, "A Numerical Method for Predicting the Cavitation Inception of a Submerged Vortex in Pump Sump," *IAHR Symposium Proceedings*, 2B-CFD-G03.
- [5] Iwano, R., Shibata, T., Nagahara, T., and Okamura, T., 2002, "Numerical Prediction Method of a Submerged Vortex and its Application to the Flow in Pump Sumps with and without a Baffle Plate," *Proceedings of the 9th International Symposium on Transport Phenomena and Dynamics of Rotating Machinery*.
- [6] Iwano, R., Shibata, T., Nagahara, T., and Okamura, T., 2002, "Development of a Numerical Method for Predicting Submerged Vortex Cavitation in a Pump Sump," *Trans. Jpn. Soc. Mech. Eng. B*, 68-667, pp. 652-657 (in Japanese).
- [7] Nagahara, T., Sato, T., and Okamura, T., 2001, "Effect of the Submerged Vortex Cavitation Occurred in Pump Suction Intake on Hydraulic Forces of Mixed Flow Pump Impeller," *Proc. 4th International Symposium on Cavitation*, B8.006.
- [8] Arndt, R. E. A., 1992, "Water Quality Effects on Cavitation Inception in Trailing Vortex," *Trans. ASME, J. Fluids Eng.*, Vol. 114, pp. 430-438.